2020 IEEE/RSJ International Conference on Intelligent Robots and Systems (IROS)
October 25-29, 2020, Las Vegas, NV, USA (Virtual)

# Design of a Highly-Maneuverable Pneumatic Soft Actuator Driven by Intrinsic SMA Coils (PneuSMA Actuator)*

Emily A. Allen[1] and John P. Swensen[1]

*Abstract*— **This paper presents the design of a new soft pneumatic actuator whose direction and magnitude of bending may be precisely controlled via activation of different shape memory alloy (SMA) springs within the actuator, in conjunction with pneumatic actuation. This design is inspired by examples seen in nature such as the human tongue, where the combination of hydrostatic pressure and contraction of intrinsic muscle groups enables precise maneuverability and morphing capabilities. Here, SMA springs are embedded in the walls of the actuator, serving as intrinsic muscles that may be selectively activated to constrain the device. The pneumatic SMA (PneuSMA) actuator demonstrates remarkable spatial controllability evidenced by testing under different pressures and SMA activation combinations. A baseline finite element model is also developed to predict the actuator deformation under different pressure and activation conditions.**

## I. INTRODUCTION

Previously, the use of robots has been limited primarily to isolated environments for assembly, industrial fabrication, bomb diffusal, or other repetitive tasks. With the recent explosion of research in the field of soft robotics, this paradigm has shifted, enabling the use of soft robots for wearable medical devices, non-invasive biomedical equipment, helper robots, and other applications that require interaction with fragile objects or beings [1]. These applications demand the design of functional robots without heavy, rigid components that could harm the subject [2], [3].

Whereas traditional robot grippers and end effectors typically consist of rigid links with motors and cable systems to control motion about prismatic or revolute joints, soft robotics applications require the elimination of heavy, rigid parts that raise safety concerns. Thus, new strategies for actuation, structural integrity, and strength capabilities must be explored within the realm of soft materials [3], [4]. Maintaining the functionality and maneuverability of traditional robots while using soft materials is a challenging task as it complicates modeling/control schema and often requires the ability to control stiffness of the materials [5], [6].

Soft pneumatic actuators use compressed air as a driving force and are a popular approach to soft robotics as they contain no rigid parts. These actuators typically consist of a rubber chamber that is pressurized to cause expansion or motion in a direction determined by geometric or external constraints [7], [8]. Several different constraint strategies have been employed to cause different types of motions [9], [10].

One of the most well-known constraint types is seen in the McKibben Pneumatic Artificial Muscles (PAM's). These actuators are encased in a woven sleeve that transmits radial expansion into longitudinal contraction [11]. These PAM's offer a high strength-to-weight ratio with contractile behavior similar to human and animal muscles [12], [13], [14], [15].

In other pneumatic actuators, expansion is directed by means of geometric constraints imposed by the rubber itself [16], [17]. In these examples, the shape of the actuator causes more resistance to stretching in certain directions, resulting in nonuniform expansion. Often this is achieved with a thick wall on one side of the actuator that resists expansion more than the other walls, causing a bending motion [18].

Some pneumatic actuators utilize separate parallel channels or tubes within a single actuator [19], [20], [21]. These channels can then be selectively activated to cause bending in different directions. Dividing the channels into individually-controlled segments further improves controllability, although stiffness is still a concern.

Other researchers incorporate fibers as strain-limiting components, where different fiber arrangements cause different types of motions such as torsion, bending, and extension [22], [23]. Particularly relevant to this work is the PneuFLEX actuator by Deimel et al. [24], where fibers wrapped radially around the actuator constrain radial expansion, and additional fibers or inextensible fabric along one side of the actuator cause substantial bending upon inflation [25]. While these actuators offer desirable deformation capabilities, their motion is limited by the arrangement of the fibers within the actuator. Fiber-reinforced bending actuators are only capable of bending in one direction, predetermined by the placement of the fibers [22]. These actuators serve well as grippers, where only one direction of motion is required, but they lack more diverse posture variability [24], [26].

The pneumatic SMA (PneuSMA) actuator proposed in this is work is capable of multi-directional bending. Here shape memory alloy (SMA) coils are embedded along different sides of the actuator to act as "smart fibers." These coils are constraints that may be selectively activated by localized heating. The combination of radially-wrapped fibers and selective activation of the SMA coils enables bending with controllable magnitude and direction. This controllability drastically expands the workspace compared to simple pneumatic bending actuators.

Actuators similar to the proposed work include SMA-driven soft actuators by Taniguchi and Alcaide et al. [27],

*This work was supported by the National Science Foundation's National Robotics Initiative Award 1734117

[1]Emily A. Allen and John P. Swensen are with the School of Mechanical and Materials Engineering, Washington State University, Pullman, WA 99164, USA emily.allen2@wsu.edu, john.swensen@wsu.edu

[28]. These actuators offer similar directional bending control via selective activation of different SMA coils. However, they incorporate air supply for the purpose of peristaltic motion or as a cooling mechanism rather than using the pneumatic pressure as a bending agonist with the SMA's as in the case of the PneuSMA actuator proposed here.

Others have employed similar dual actuation strategies, using tendons to control the bending direction of pneumatic actuators with activation of antagonistic groups enabling a high stiffness state [29], [30]. While these designs offer similar spatial controllability and stiffness control, they incorporate separate tendons for each independently-controlled segment of the actuator, whereas the PneuSMA actuator includes only one SMA spring along each bending direction and does not suffer friction and undesirable force transmission from distal tendons. Different segments of a single SMA coil may be activated in the PneuSMA actuator to control bending in any segment of the actuator independently. In tendon-driven actuators, proximal segments are adversely affected when distal tendons are pulled.

## II. MATERIALS AND METHODS

### A. Actuator Design

The design of the PneuSMA Actuator shown in Fig. 1 is inspired by the PneuNet and PneuFLEX continuous actuators which are capable of bending tightly upon pressurization. While the PneuNet and PneuFLEX actuators use only fibers as geometric constraints, the PneuSMA actuator incorporates both fibers and SMA coils which serve as constraints that may be selectively activated to offer precise spatial control.

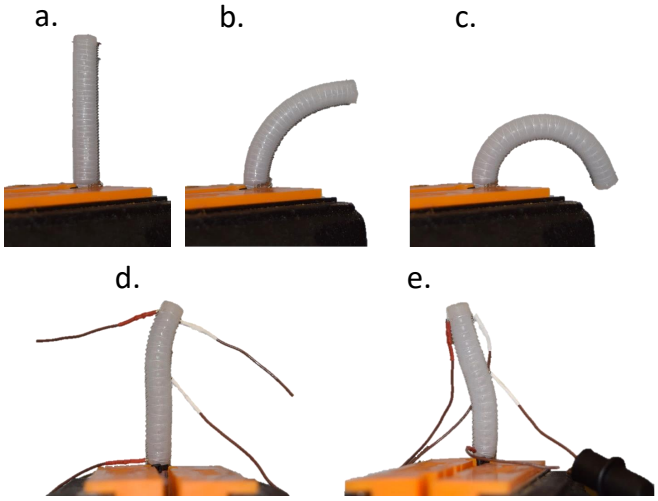


Fig. 1. Controlled deformation capabilities of PneuSMA actuator. (a)-(c) show the bending of a PneuSMA actuator with 2 side-by-side SMA coils embedded along the right side, with increasing internal pressure from left to right. (d) and (e) show selective activation of coil segments along both the left and right sides of the actuator.

The design of this actuator exploits the principle of anisotropic elasticity. Fibers wrapped helically along the length of the actuator prevent radial expansion, thus forcing longitudinal elongation. The SMA coils along the sides hinder elongation of one side of the actuator when activated by a heat stimulus. Due to the shape memory effect, the pre-stretched SMA coils exert a shortening force along one side of the actuator when heated via electrical current. Meanwhile, the rest of the actuator extends longitudinally due to the internal pressure and radial constraint. The combination of internal pressure and SMA spring force causes substantial bending of the actuator. As shown in Fig. 1, the actuator may be controlled by heating different segments of the coils.

### B. Actuator Fabrication

Fabrication of the actuator requires minimal supplies and equipment. Dragon Skin$^{TM}$ 20 Silicone was used for the main body of the actuator. The other assembly materials include polyester thread, 4mm x 6mm PVC tubing, 0.25mm x 0.9mm Nitinol micro spring (tight pitch), 3D printed ABS mold and core, Sil-Poxy silicone glue, and a small cable tie.

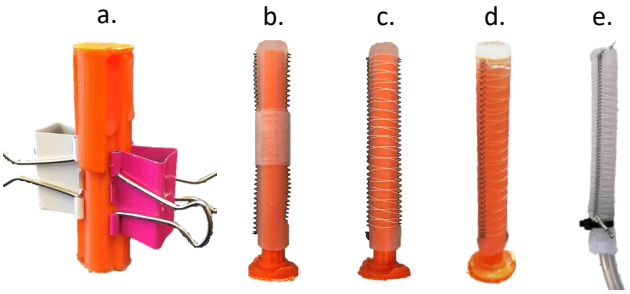


Fig. 2. PneuSMA Actuator fabrication steps including (a) casting of silicone tube, (b) placement of pre-stretched Nitinol coils, (c) wrapping of the radial fibers around SMA springs, (d) thin coating of silicone over fibers, and (e) completed actuator.

To assemble the actuator, the plastic mold pieces are sprayed with Mold-Release spray to prevent adhesion of the silicone to the mold. The liquid silicone parts A and B are mixed together in equal parts by mass then degassed in a vaccuum chamber. As shown in Fig. 2 (a), the outer mold pieces are then clamped together and filled with the prepared liquid silicone before the plastic core is inserted. The outer mold pieces are removed once the silicone has cured for at least 4 hours. Next, the Nitinol coils are pre-stretched to 4 times their original length. This 300% spring strain corresponds to about 6% strain of the Nitinol material. The coils are then positioned along the sides of the silicone and temporarily secured with tape. As shown in Fig. 2 (c), the thread fiber is wrapped in a double helix pattern around the actuator with one thread passing between each coil of the Nitinol. The thread is wrapped spirally starting from the tip, skipping every other coil. Then once wrapped all the way to the base, the wrapping continues spirally outward, back to the tip, passing through each of the skipped coils. The two ends of the threads are then tied together and trimmed. To secure the fibers in place, a second layer of liquid silicone is spread thinly over the fibers and coils as seen in Fig. 2 (d). Once cured, the plastic core is removed, and the PVC tubing is inserted in the opening. A small amount of silicone glue and a cable tie seal the opening around the supply tube.

### C. Test Setup and Procedure

In this work, testing of the actuators is designed for the following objectives:

- Demonstrate spatial controllability enabled by selective activation of different coil segments.
- Assess effectiveness of multiple SMA coils in increasing actuator curvature.
- Compare bending behavior of SMA-driven PneuSMA actuator with that of purely fiber-reinforced actuator.
- Compare static FEA model with experimentally-measured actuator curvatures.

To assess these objectives, five different actuators were constructed as shown in Fig. 3. Actuators (a) and (b) respectively have 1 and 2 side-by-side coils along one side of the actuator. Actuator (c) has no SMA coils but instead has a Nylon fiber embedded along one side of the actuator to serve as an inextensible constraint. Actuator (d) has one coil along each side of the actuator with conductive wires attached at different locations along the coils for selective heating. Actuators (a) - (d) have an outer diameter of 10 mm. Actuator (e) has one SMA spring along one side and has a smaller overall diameter than the others (6mm). The test setup is shown in Fig. 3 (f) with the actuator clamped in a vice with the supply tube attached to a large syringe. A force cell attached to a Mark10 test stand is lowered to compress the plunger in the syringe and pressurize the actuator.

During testing, the force cell is lowered continuously on the syringe, gradually pressurizing the actuator. Side-view photos are captured to record the deformed shape of the actuator as the pressure increases. These photos are analyzed afterwards to determine the bend radius of the actuator, and the corresponding force on the syringe is used to calculate the internal pressure based on the area of the plunger.

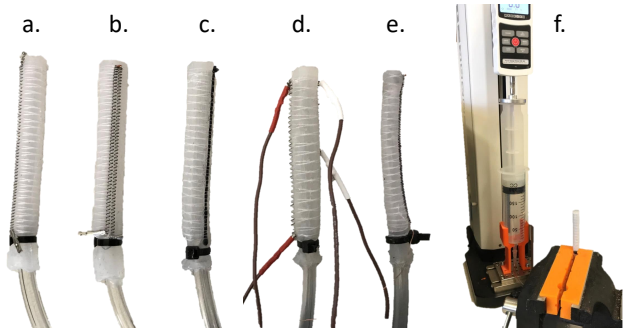


Fig. 3. Fabricated samples and bend test setup. Actuators (a) and (b) contain 1 and 2 side-by-side coils along one side; actuator (c) contains a nylon fiber along one side; actuator (d) contains one coil along each side; and actuator (e) contains a single coil on one side and has a smaller diameter.

### D. Finite Element Modeling

The bending of the PneuSMA actuator is described using a simplified modeling approached based on the stiffness of the silicone rubber and finite element analysis of parallel springs along the length of the actuator as shown in Figs. 4 and 5. In modeling the bending of a PneuSMA actuator

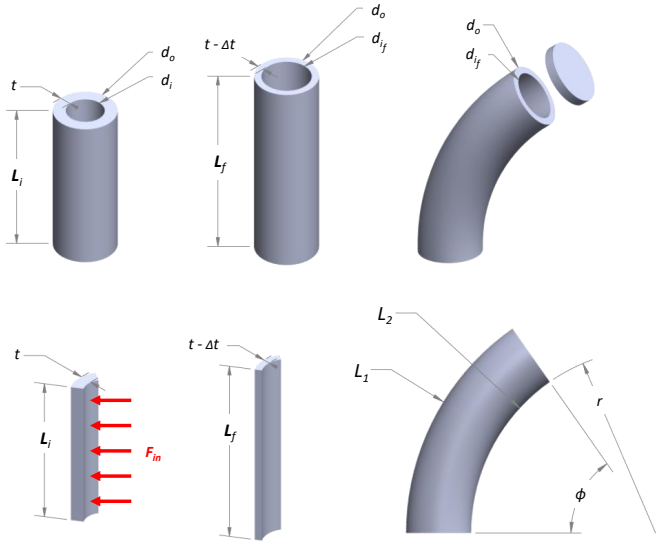


Fig. 4. PneuSMA actuator dimensions and modeling steps.

with SMA coils along one side only, we begin by accounting for the lengthening of the actuator due to the pressure on the inside walls of the actuator. This elongation and the related dimmensions are shown in Fig. 4. The outside walls of the actuator are assumed to be fixed at a constant diameter since the close-packed helical fibers prevent significant radial expansion. The silicone rubber has a Poisson's ratio of 0.47 - 0.49 reported in the literature, indicating that the material is nearly incompressible. Thus, it is reasonable to assume that any compression of the inner walls results in elongation of the actuator if we impose a constant volume constraint on the silicone material. The change in thickness of the actuator walls $\Delta t$ can be expressed using the nonlinear stiffness of the silicone material to describe the compression:

$$F_{in} = PA_{in} = \frac{EA_{in}}{t}\Delta t \quad \Rightarrow \quad \Delta t = \frac{Pt}{E}, \qquad (1)$$

where $A_{in}$ is the surface area of the inner walls of the actuator, $E$ is the secant modulus of the silicone, and $P$ is the internal pressure. The resulting length of the actuator can then be calculated as a function of pressure by imposing the silicone constant volume constraint:

$$L_f = \frac{A_{initial}}{A_{final}} L_i = \frac{d_o^2 - d_i^2}{d_o^2 - (d_o - 2[t - \frac{Pt}{E}])^2} L_i, \qquad (2)$$

where $A_{initial}$ and $A_{final}$ refer to the annular cross-sectional area of the actuator before and after pressurization. The force on the walls of the actuator due to the internal pressure is thus transmitted to the longitudinal direction. This longitudinal force responsible for the actuator elongation can be calculated by

$$F_{el} = A_{final}\, E\, \frac{L_f - L_i}{L_i}. \qquad (3)$$

The force on the end cap of the actuator due to internal pressure is simply

$$F_{end} = P\frac{\pi}{4}d_{if}^2 = P\frac{\pi}{4}(d_o - 2[t - \Delta t])^2. \qquad (4)$$

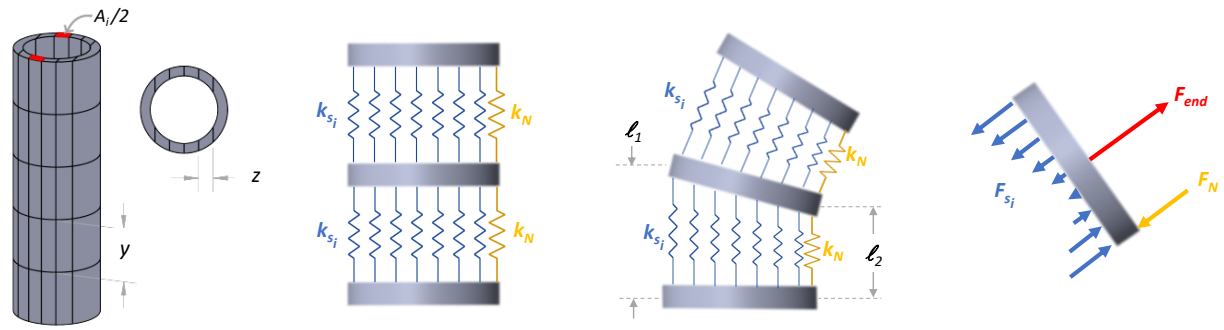


Fig. 5. Schematic discretization of PneuSMA actuator for finite element analysis where forces acting on the end of the actuator are shown on the right.

The total external force acting in the longitudinal direction is simply the sum of the elongation force and the force on the end of the actuator:

$$F_{ext} = F_{el} + F_{end} \tag{5}$$

Now to account for the actuator bending, we discretize the actuator to model the bending stiffness of the silicone and the tensile force of the Nitinol as a system of springs as shown in Fig. 5. The actuator is divided into $m$ segments along its length and $p$ segments along its width, resulting in $m * p$ total springs representing the silicone, in addition to $m$ springs along the right side to model the Nitinol spring force. A zero displacement boundary condition exists at the base of the actuator where it is clamped in the vice, and the external force $F_{ext}$ acts on the last segment of the actuator due to the internal pressure acting on the end of the actuator.

The nonlinear stiffness of each silicone spring element depends on the silicone secant modulus $E$, the rest length of the spring $\ell_{0_s}$, and the effective area of each spring $A_i$:

$$k_{s_i} = \frac{EA_i}{\ell_{0_s}}. \tag{6}$$

As seen in Fig. 5, the rest lengths of all silicone spring elements are identical, but the effective area varies along the width of the actuator due to the annular cross section. Thus, all springs in series have the same stiffness, but parallel springs have different stiffness values. The rest length of each of the silicone springs is simply

$$\ell_{0_s} = \frac{L_i}{m}, \tag{7}$$

where $m$ is the number of spring segments in series. The Nitinol nonlinear spring stiffness was measured experimentally in the Austenite phase for incorporation in the model. Note that the rest length of the Nitinol spring elements is not the same as the rest length of the silicone spring elements. Becuase the Nitinol coils were prestretched before being attached to the actuator, they have a much shorter rest length.

Assuming that each set of parallel springs stretches or compresses to some new length $\ell_1$ on the left side of the actuator and $\ell_2$ on the right side, the tensile force in each Nitinol spring element can be expressed as

$$F_N = k_N(\ell_2 - \ell_{0_N}), \tag{8}$$

where $\ell_{0_N}$ is the rest length of each Nitinol spring element. The tensile force in each silicone spring element can then be expressed as

$$F_{s_i} = k_{s_i}(\ell_i - \ell_{0_s}), \tag{9}$$

where $\ell_i$ is the length of the $i^{th}$ spring element, determined by linear interpolation between $\ell_1$ and $\ell_2$ shown in Fig. 5. Here a negative force indicates compression.

The resulting shape of the actuator is determined by varying the element stretch lengths $\ell_1$ and $\ell_2$ until a static force and moment balance is achieved, including the external force $F_{ext}$. The radius of curvature $r$ from Fig. 4 is defined using the sum of the element side lengths:

$$\kappa = \frac{1}{r} = \frac{L_1/L_2 - 1}{d_o} = \frac{\sum \ell_1 / \sum \ell_2 - 1}{d_o}. \tag{10}$$

## III. RESULTS AND DISCUSSION

### A. Precise Spatial Maneuverability

The PneuSMA actuator demonstrated overall precise spatial maneuverability enabled by the selective actuation of different coil segments. Fig. 1 (a) through (c) show the bending of actuator (b) which contains two side-by-side SMA coils along the right side. Here the bend radius is controlled by the pressure applied to the actuator supply, and an increase in pressure causes tighter bending as seen in Fig. 1 (c). Fig. 1 (d) and (e) show the deformation of actuator (d) which contains one SMA coil along each side. In Fig. 1 (d), the top section only of the right coil is heated while the left coil and the bottom of the right coil remain at room temperature. This causes localized bending to the right precisely at the tip of the actuator. In Fig. 1 (e), the entire length of the left side coils are heated as well as the upper half of the right side coils. The bottom half of the right side coils remain at room temperature, allowing bending to the left precisely at the base of the actuator.

Fig. 6 shows the maneuverability of the narrow actuator (e) which can achieve a tight bend radius, even wrapping around an 8mm pen. Its narrow body enables tight curvature and proves that these actuators can be scaled down for use in space-constrained medical applications. In Fig. 6 (b) and (c), different segments of the SMA spring is activated to cause precise control of distal and proximal bending, respectively.

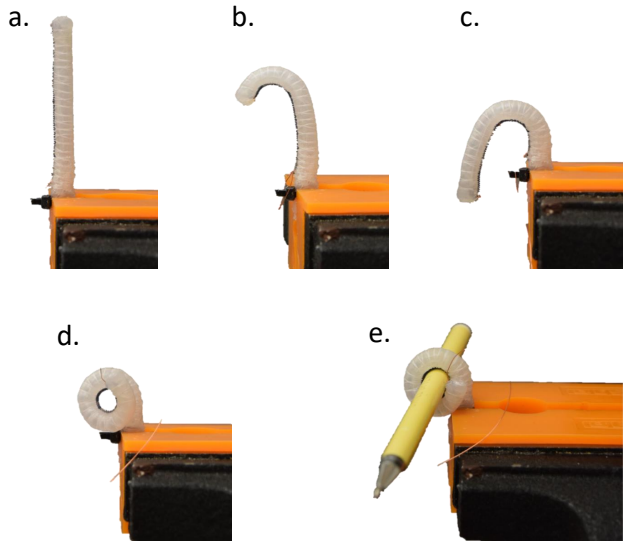


Fig. 6. Demonstrated spatial maneuverability and tight curvature with narrow PneuSMA actuator.

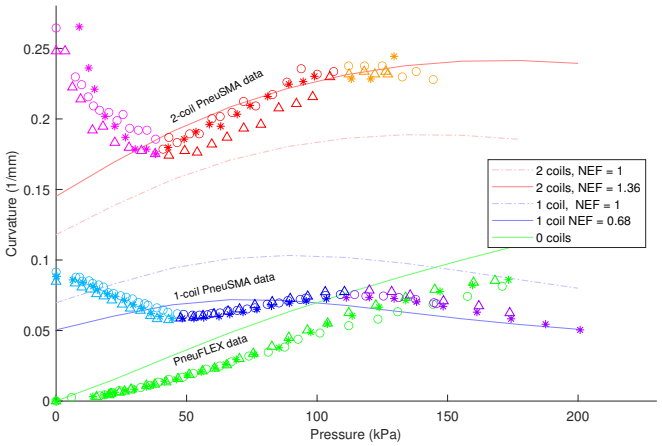


Fig. 7. Comparison of FEA model with measured bending behavior.

### *B. Tighter Bending with Multiple Side-By-Side Coils*

Actuators (a), (b), and (c) were tested at a variety of pressures while the coils were fully activated to assess the effectiveness of additional coils to increase the curvature at any given pressure. The data points in Fig. 7 show the curvature measured for each of the three actuators at different pressures. The bend data shows higher curvature in the PneuSMA actuators with more coils for any given pressure. Thus, additional coils enable tighter bending of the actuator.

The green data points in Fig. 7 show the measured curvature of the fibers-only actuator, actuator (c). The blue/purple data series shows measured curvatures from the PneuSMA actuator (a) with one Nitinol spring along the entire length of one side of the actuator. The pink/red/orange data series shows measured curvatures from the PneuSMA actuator (b) with two side-by-side coils along the entire length of one side of the actuator. Overall, the PneuSMA actuators exhibit significantly higher curvatures than the PneuFLEX actuator (c). At low pressures, the SMA-driven actuator (a) outperforms the fiber-only actuator, but at pressures above about 140 kPa, the opposite is true. This makes sense since the SMA coils are not inextensible; they can offer some compression at low pressures but also suffer some elongation at high pressures. Thus, the PneuSMA actuators should be designed for use at moderate pressures, below the curvature plateau around 120 kPa.

### *C. Modeling Results*

The static finite element model was tested against experimental data from the 3 different actuators. A comparison of the measured curvatures and model-predicted curvatures is shown in Fig. 7. The curvatures predicted by the finite element model are shown by the solid curves. The model-predicted curvatures generally match the trends of the experimental data, but evidence some discrepancy. A Nitinol Effectiveness Factor (NEF) has been included in the model to account for assumed restraints on the Nitinol coils that prevent compression of the springs and reduce the overall shortening force exerted by the springs. This factor is essentially a curve-fitting parameter. The NEF should hold consistent between both the 1-coil and 2-coil PneuSMA actuators unless the errors are attributed to fabrication inconsistencies. From Fig. 7, it can be seen that the NEF's required to fit the experimental data are not the same between the 1-coil and 2-coil actuator. The model fits the data best with an NEF of 0.68 and 1.36 for the 1-coil and 2-coil data, respectively. This suggests possible inconsistencies in the samples tested or a physical principle not accounted for in the model.

At low pressures (below about 45 kPa), the PneuSMA actuators buckle when the SMA coils are activated because the low internal pressure is insufficient to prevent the actuator from collapsing on itself under the compressive force from the coils. The FEA model does not account for buckling, so this unstable behavior is not matched by the model. This buckling behavior explains the deviation between the model and data at low pressures in Fig. 7. Although it complicates modeling, the silicone buckling introduced by the SMA contraction is actually beneficial as it enables much tighter bending than is possible with the simple PneuFLEX actuator which does not facilitate any buckling. When the silicone material buckles, it does not exert as much force as the thick silicone compression test samples, so a different modeling approach will be required for this type of behavior. Modeling the silicone force in buckling may involve estimated constant force modeling or incorporation of experimentally measured force exerted by a buckled actuator in compression.

Additional testing should also be conducted on a PneuSMA actuator with discrete segments of the SMA coils activated. This will produce unique configurations that no longer classify as constant curvature. The proposed finite element model should then be compared with these results to ensure that the model holds true for more advanced manipulations.

## IV. CONCLUSION

We presented the novel design of a pneumatic soft actuator with embedded SMA coils that serve as intrinsic muscle fibers to direct the deformation. Different segments along the actuator may be independently controlled by heating select SMA spring segments, eliminating the need to lengthy tendon routes. The actuator demonstrated highly dexterous capabilities that make it well-suited for soft end effectors that operate in fragile environments requiring precise maneuverability. The actuators can be made as thin as 6mm, bending with a radius of curvature down to 4mm. The actuator is entirely biocompatible and may lend itself well to biomedical devices such as catheters or colonoscopes. Adapting the design for these types of applications will require making the actuator thinner than the current 10 mm and 6 mm designs and embedding the SMA springs internally where the heat activation would be shielded from surrounding tissue. A pneumatic venting system could then dissipate heat from the internal SMA coils. The actuator may be further improved by including more intrinsic muscles to enable even finer control.

## REFERENCES


[1] M. Runciman, A. Darzi, and G. P. Mylonas, "Soft robotics in minimally invasive surgery," *Soft robotics*, vol. 6, no. 4, pp. 423–443, Aug 2019. [Online]. Available: https://www.ncbi.nlm.nih.gov/pubmed/30920355

[2] C. Laschi, B. Mazzolai, and M. Cianchetti, "Soft robotics: Technologies and systems pushing the boundaries of robot abilities," *Science Robotics*, vol. 1, no. 1, 2016.

[3] C. Majidi, "Soft robotics: A perspectivecurrent trends and prospects for the future," *Soft Robotics*, vol. 1, no. 1, pp. 5–11, 2014. [Online]. Available: https://doi.org/10.1089/soro.2013.0001

[4] A. Miriyev, G. Caires, and H. Lipson, "Functional properties of silicone/ethanol soft-actuator composites," *Materials & Design*, vol. 145, pp. 232 – 242, 2018. [Online]. Available: http://www.sciencedirect.com/science/article/pii/S0264127518301485

[5] G.-Z. Yang, J. Bellingham, P. E. Dupont, P. Fischer, L. Floridi, R. Full, N. Jacobstein, V. Kumar, M. McNutt, R. Merrifield, B. J. Nelson, B. Scassellati, M. Taddeo, R. Taylor, M. Veloso, Z. L. Wang, and R. Wood, "The grand challenges of science robotics," *Science Robotics*, vol. 3, no. 14, 2018. [Online]. Available: http://robotics.sciencemag.org/content/3/14/eaar7650

[6] S. Kim, C. Laschi, and B. Trimmer, "Soft robotics: a bioinspired evolution in robotics," *Trends in Biotechnology*, vol. 31, no. 5, pp. 287 – 294, 2013. [Online]. Available: http://www.sciencedirect.com/science/article/pii/S0167779913000632

[7] P. Beyl, M. Van Damme, R. Van Ham, B. Vanderborght, and D. Lefeber, "Pleated pneumatic artificial muscle-based actuator system as a torque source for compliant lower limb exoskeletons," *Mechatronics, IEEE/ASME Transactions on*, vol. 19, no. 3, pp. 1046–1056, 2014.

[8] Y. Li, Y. Chen, T. Ren, Y. Li, and S. h. Choi, "Precharged pneumatic soft actuators and their applications to untethered soft robots," *Soft Robotics*, vol. 5, no. 5, pp. 567–575, 2018, pMID: 29924683. [Online]. Available: https://doi.org/10.1089/soro.2017.0090

[9] D. Rus and M. Tolley, "Design, fabrication and control of soft robots," *Nature*, vol. 521, no. 7553, pp. 467–475, 2015.

[10] A. D. Marchese, R. K. Katzschmann, and D. Rus, "A recipe for soft fluidic elastomer robots," *Soft Robotics*, vol. 2, no. 1, pp. 7–25, 2015, pMID: 27625913. [Online]. Available: https://doi.org/10.1089/soro.2014.0022

[11] J. D. W. Madden, N. A. Vandesteeg, P. A. Anquetil, P. G. A. Madden, A. Takshi, R. Z. Pytel, S. R. Lafontaine, P. A. Wieringa, and I. W. Hunter, "Artificial muscle technology: physical principles and naval prospects," *IEEE Journal of Oceanic Engineering*, vol. 29, no. 3, pp. 706–728, July 2004.

[12] F. Daerden and D. Lefeber, "Pneumatic artificial muscles: actuators for robotics and automation," *European journal of mechanical and environmental engineering*, vol. 47, no. 1, pp. 11–21, 2002.

[13] T. Doi, S. Wakimoto, K. Suzumori, and K. Mori, "Proposal of flexible robotic arm with thin mckibben actuators mimicking octopus arm structure," in *2016 IEEE/RSJ International Conference on Intelligent Robots and Systems (IROS)*, Oct 2016, pp. 5503–5508.

[14] S. Furukawa, S. Wakimoto, T. Kanda, and H. Hagihara, "A soft master-slave robot mimicking octopus arm structure using thin artificial muscles and wire encoders," *Actuators*, vol. 8, p. 40, 05 2019.

[15] D. Villegas Casi, M. Van Damme, B. Vanderborght, P. Beyl, and D. Lefeber, "Third generation pleated pneumatic artificial muscles for robotic applications: Development and comparison with mckibben muscle," *Advanced Robotics*, vol. 26, no. 11-12, pp. 1205–1227, 7 2012.

[16] B. Gorissen, D. Reynaerts, S. Konishi, K. Yoshida, J.-W. Kim, and M. De Volder, "Elastic inflatable actuators for soft robotic applications," *Advanced Materials*, vol. 29, p. 1604977, 09 2017.

[17] G. M. Whitesides, "Soft robotics," *Angewandte Chemie International Edition*, vol. 57, no. 16, pp. 4258–4273, 2018. [Online]. Available: https://onlinelibrary.wiley.com/doi/abs/10.1002/anie.201800907

[18] R. Praneeth, N. S. Kiran, S. Aditya, K. Anjai, S. Pramod, and G. Udupa, "Design, analysis, manufacturing and testing of artificial hand with fingers made of rubber actuators," *Materials Today: Proceedings*, vol. 5, no. 11, Part 3, pp. 25 236 – 25 244, 2018. [Online]. Available: http://www.sciencedirect.com/science/article/pii/S2214785318326300

[19] F. Ilievski, A. D. Mazzeo, R. F. Shepherd, X. Chen, and G. M. Whitesides, "Soft robotics for chemists," *Angewandte Chemie*, vol. 123, no. 8, pp. 1930–1935, 2011.

[20] R. V. Martinez, J. L. Branch, C. R. Fish, L. Jin, R. F. Shepherd, R. M. D. Nunes, Z. Suo, and G. M. Whitesides, "Robotic tentacles with three-dimensional mobility based on flexible elastomers," *Advanced Materials*, vol. 25, no. 2, pp. 205–212, 2013. [Online]. Available: https://onlinelibrary.wiley.com/doi/abs/10.1002/adma.201203002

[21] Y.-F. Zhang, C. J.-X. Ng, Z. Chen, W. Zhang, S. Panjwani, K. Kowsari, H. Y. Yang, and Q. Ge, "Miniature pneumatic actuators for soft robots by high-resolution multimaterial 3d printing," *Advanced Materials Technologies*, vol. 0, no. 0, p. 1900427. [Online]. Available: https://onlinelibrary.wiley.com/doi/abs/10.1002/admt.201900427

[22] F. Connolly, P. Polygerinos, C. Walsh, and K. Bertoldi, "Mechanical programming of soft actuators by varying fiber angle," *Soft Robotics*, vol. 2, no. 1, pp. 26–32, 3 2015.

[23] J. Bishop-Moser, G. Krishnan, C. Kim, and S. Kota, "Design of soft robotic actuators using fluid-filled fiber-reinforced elastomeric enclosures in parallel combinations," in *2012 IEEE/RSJ International Conference on Intelligent Robots and Systems*, Oct 2012, pp. 4264–4269.

[24] R. Deimel and O. Brock, "A compliant hand based on a novel pneumatic actuator," *2013 IEEE International Conference on Robotics and Automation*, pp. 2047–2053, 2013.

[25] P. Polygerinos, Z. Wang, J. T. B. Overvelde, K. C. Galloway, R. J. Wood, K. Bertoldi, and C. J. Walsh, "Modeling of soft fiber-reinforced bending actuators," *IEEE Transactions on Robotics*, vol. 31, no. 3, pp. 778–789, June 2015.

[26] R. Deimel and O. Brock, "A novel type of compliant and underactuated robotic hand for dexterous grasping," *The International Journal of Robotics Research*, vol. 35, no. 1-3, pp. 161–185, 2016. [Online]. Available: https://doi.org/10.1177/0278364915592961

[27] H. Taniguchi, "Flexible artificial muscle actuator using coiled shape memory alloy wires," *APCBEE Procedia*, vol. 7, pp. 54 – 59, 2013, the 3rd International Conference on Biomedical Engineering and Technology - ICBET 2013. [Online]. Available: http://www.sciencedirect.com/science/article/pii/S2212670813001140

[28] J. O. Alcaide, L. Pearson, and M. Rentschler, "Design, modeling and control of a sma-actuated biomimetic robot with novel functional skin," *2017 IEEE International Conference on Robotics and Automation (ICRA)*, pp. 4338–4345, 2017.

[29] F. Maghooa, A. Stilli, Y. Noh, K. Althoefer, and H. A. Wurdemann, "Tendon and pressure actuation for a bio-inspired manipulator based on an antagonistic principle," in *2015 IEEE International Conference on Robotics and Automation (ICRA)*, May 2015, pp. 2556–2561.

[30] A. Shiva, A. Stilli, Y. Noh, A. Faragasso, I. D. Falco, G. Gerboni, M. Cianchetti, A. Menciassi, K. Althoefer, and H. A. Wurdemann, "Tendon-based stiffening for a pneumatically actuated soft manipulator," *IEEE Robotics and Automation Letters*, vol. 1, no. 2, pp. 632–637, July 2016.